Optical-Comb-Based Frequency Stability Transfer Across the Spectrum With a Multichannel FPGA

Optical-Comb-Based Frequency Stability Transfer Across the Spectrum With a Multichannel FPGA

Paolo Savio, Irene Goti, Marco Pizzocaro, Filippo Levi, Davide Calonico, and Cecilia Clivati

***Abstract*—Using the optical comb as a transfer oscillator is an effective approach to convert the spectral properties of ultrastable lasers to other wavelength domains. We describe a digital locking system that enables this process to be replicated for several lasers at a time, supporting the simultaneous and independent lock of up to six lasers to a single, high-performance reference oscillator. The locks are robust, easily reconfigured, and contribute a short-term instability lower than 3×10^{-18} at 1 s, even when the comb is operated in the broad-linewidth regime and with no need for lasers prestabilization. With this system, we transfer the coherence of the ultrastable clock laser of a Yb optical lattice clock at 1156 nm to various lasers in the 1550 nm region, including the one used for frequency dissemination with long-distance fibers, with less than 1×10^{-17} instability at 1 s. The digital implementation enables a modular approach with enhanced control over operational parameters, minimizing setup complexity and hardware-related undesired effects. It also allows for immediate reconfiguration and seamless upgrades, being suitable for applications requiring multiple ultrastable lasers at different wavelengths, such as local or distributed optical clock ensembles, coherent spectroscopy, and quantum simulation.**

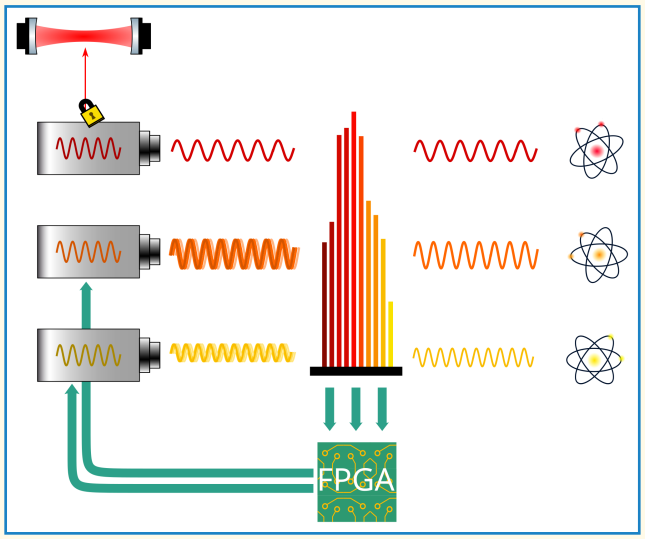

***Index Terms*—Field-programmable gated array (FPGA), low-noise frequency synthesis, optical frequency comb, ultrastable lasers.**

I. Introduction

ULTRASTABLE lasers are crucial ingredients in a wide variety of experimental fields, from gravitational waves interferometry [1] to quantum communication [2] and simulation [3], fundamental physics and metrology. Optical clocks rely on lasers with frequency instability of 10^{-16} and below to achieve uncertainties of 10^{-18} in 1 h of integration time [4], [5], in turns supporting the generation of advanced timescales [6], [7], [8], [9] in the frame of the forthcoming redefinition of the second [10], [11], chronometric leveling with cm-level resolution [12], [13], [14], [15], and advanced tests of fundamental physics both at local [16], [17] or distributed scale [18].

Received 16 September 2024; accepted 3 January 2025. Date of publication 7 January 2025; date of current version 17 March 2025. This work was supported by project 20FUN08 Nextlasers, that has received funding from the EMPIR programme co-financed by the Participating States and from the European Union's Horizon 2020 research and innovation programme. *(Corresponding author: Cecilia Clivati.)*

Paolo Savio is with Fondazione LINKS, 10134 Turin, Italy (e-mail: paolo.savio@linksfoundation.com).

Irene Goti, Marco Pizzocaro, Filippo Levi, Davide Calonico, and Cecilia Clivati are with Istituto Nazionale di Ricerca Metrologica—INRIM, 10135 Turin, Italy (e-mail: c.clivati@inrim.it).

Digital Object Identifier 10.1109/TUFFC.2025.3526761

Today, ultrastable lasers are mostly realized by active stabilization to high-finesse resonators with low-thermal noise mirrors and extreme environmental isolation, and achieve frequency stability up to parts in 1×10^{-17} [19], [20]. Their realization, characterization [21], and maintenance require sophisticated and costly instrumentation, dedicated expertise and continued effort. In some cases, solutions are wavelength-specific and their replication in different spectral domains is hence not practical.

Thanks to its broadband spectrum, the optical comb enables to convert the spectral properties of a single, superior reference laser to other wavelengths with no degradation [22]. This concept can be implemented either by operating the comb in the narrow-linewidth regime [23], or by using it as a transfer oscillator [24], [25], [26]. The latter approach has the advantage of preserving the absolute traceability, enabling the comb to be referenced by a radio frequency (RF) standard, while rejecting its fast fluctuations to the highest level.

Hardware implementation of the transfer oscillator concept relies on analog components such as mixers and direct digital synthesizers (DDSs) and often includes amplifiers, filters, additional mixing stages and tracking-oscillator filters to satisfy minimum signal/noise ratio (SNR) requirements [25],

Highlights

- **We describe a digital system for implementing frequency stability transfer using the comb as a transfer oscillator, showing that up to six laser can be independently locked to a common reference.**
- **We characterize our FPGA-based system and demonstrate stability transfer between 1156 and 1542 nm with $<1 \times 10^{-17}$ instability at 1 s and 200 kHz bandwidth.**
- **This system allows generation of coherent radiation across the spectrum, with applications to optical clock ensembles, high-resolution spectroscopy, and quantum technologies.**

[26], [27]. Digital electronics is a viable alternative, offering advantages such as high reproducibility, controllable operational parameters, minimization of hardware components, and modular replication to simultaneously lock several lasers.

In the past decade, field-programmable gated arrays (FPGAs) have been progressively introduced in the frequency metrology community for phase noise analysis of oscillators [28], [29], [30], fiber stabilization [31], [32], [33], synchronous optical measurements [34], [35], and stabilization of optical combs [36], [37], [38]. In many of those applications, it is important to comply with metrological requirements in terms of accuracy and support robust and cycle-slip-free locks of optical oscillators having typical phase noise in excess of 10^2 rad^2 in ms-long integration time. These aspects call for careful analysis of bandwidth, latency, and resolution concerns, in turns set by the sampling rate, algorithm complexity, and effective number of bits in the employed logic.

In this article, we describe a multichannel FPGA board for the implementation of the transfer oscillator concept, where several lasers at different wavelengths are all made coherent to a single reference laser. After recalling the principle of the transfer oscillator and its digital implementation, we will report on the outcome of experimental tests quantifying both the noise contributed by the FPGA board alone and by the entire spectral conversion process. The developed system supports the simultaneous lock of up to six lasers, considerably reducing the setup complexity and enabling a single, superior laser to serve independent experiments. As a use case, we demonstrate the frequency stability transfer between a Yb optical clock laser at 1156 nm to lasers in the 1550 nm region, which is useful in view of realizing distributed clock networks connected by phase-stabilized fiber links. The same scheme could be exploited locally to overcome the quantum projection noise limit in clock ensembles [4], [39] and develop complex atom interrogation schemes. More in general, it could find application in experiments where the laser coherence time is critical, such as quantum communication [40] and quantum simulations [3].

II. Digital Implementation of the Transfer Oscillator Concept

The digital implementation of the transfer oscillator concept is based on the synchronous measurement of the beatnotes between the two lasers being compared and the closest comb teeth. This approach leverages the fact that frequency fluctuations of the comb are common for the two beatnotes and effectively cancel out in the comparison [24]. Briefly, we assume the two lasers (hereafter, main and secondary) have frequency ν_m and ν_s described by the usual comb equation [22]

$$\begin{aligned} \nu_m &= N_m f_{\text{rep}} + f_0 + f_{b,m} \\ \nu_s &= N_s f_{\text{rep}} + f_0 + f_{b,s} \end{aligned} \tag{1}$$

where f_{rep} is the comb repetition rate, f_0 the carrier-to-envelope offset frequency, $f_{b,m}$ and $f_{b,s}$ are the frequencies of the beatnotes of the two lasers with the closest comb tooth of order N_m and N_s.

RF beatnotes at f_0, $f_{b,m}$ and $f_{b,s}$ are combined to generate a new RF signal with frequency f_T, usually known as transfer beatnote

$$f_T = \left(f_0 + f_{b,m}\right) - \frac{N_m}{N_s}\left(f_0 + f_{b,s}\right) = \nu_m - \frac{N_m}{N_s}\nu_s \tag{2}$$

where the last equivalence has been obtained by combination with (1). It is straightforward to see that fluctuations in ν_m and ν_s are mapped into fluctuations of f_T, those of ν_s with a scaling term N_m/N_s that accounts for the spectral separation from ν_m, while fluctuations in comb parameters f_{rep} and f_0 are rejected from the measurement.

The same equivalence can be applied to the respective phase fluctuations, which are the integral of instantaneous frequencies measured over the sampling interval

$$\varphi_T = \left(\varphi_0 + \varphi_{b,m}\right) - \frac{N_m}{N_s}\left(\varphi_0 + \varphi_{b,s}\right). \tag{3}$$

While in a hardware implementation, the algebraic operations of sum, difference, and scaling contained in (2) or (3) are performed with analog mixers and prescalers or DDSs [25], [26], in a digital implementation, the three beatnotes are first sampled by analog/digital converters (ADCs), and then numerically processed by a FPGA.

In our system, the digital signal processing consists of three main blocks: first, phase fluctuations of individual beatnotes are extracted; then, they are combined to fulfill (3), producing a signal which is proportional to the phase fluctuations of the secondary laser relative to the main. Finally, this information is turned into a physical signal by a digital/analog converter (DAC) and used to phase-lock the secondary laser to the main via a proportional–integral–derivative (PID) control loop. In the rest of this section, we describe in detail peculiar aspects of our implementation. As a general approach, we relied on available libraries wherever possible, while others were specifically designed for our application (e.g., the unwrap

function described later). The code we developed and to which we will refer throughout the work is freely available [41].

A. Hardware

Our implementation is based on a Zynq UltraScale+ RF System on Chip ZCU208 by AMD-Xilinx, featuring a 5 GS/s ADC and a 10 GS/s DAC, each with eight parallel channels and 14 bits of vertical resolution, 50 Mb on-chip memory and 8 GB external memory (DDR4) connected to the embedded ARM processor and to the programmable section of the FPGA. The board kit comes with an external clock generation daughterboard (CLK104), used to reference the ADC and DAC sampling clocks to an external 10 MHz signal, and a BALUN board XM655 that passively interfaces on-chip ADC/DAC pins to 50 Ω single-ended inputs/outputs. On the software side, the PYNQ package (v3.0.1) is running on the embedded processor, allowing real-time algorithm debug, raw data download, and partial board reconfiguration with a dedicated and user-friendly Python code and Jupyter notebook.

B. Sampling

Beatnote signals at $f_{b,m}$, $f_{b,s}$, and f_0 are loosely bandpass-filtered, amplified, and then sampled. Additional beatnotes can be sampled, e.g., to lock additional lasers to the same reference laser. The ADC sampling rate is preferably set to $f_s \geq f_{\text{rep}}$ to avoid aliasing, even though operating in higher Nyquist zones is possible [32], as well as working with $f_s = f_{\text{rep}}$ to improve the SNR by gated detection [42]. In this latter case, photodiodes and ADCs with minimum bandwidth of several f_{rep} are required, and the initial bandpass filters are removed. The employed board supports a minimum sampling rate of 1 GHz. We arbitrarily set it to 4 GHz (16 times the repetition rate f_{rep}) and down-sampled recorded data using the built-in decimation filters.

C. Phase Extraction

To retrieve the phase fluctuations of each sampled beatnote in real-time we employ in-phase/quadrature (I/Q) demodulation, a common approach to phase detection in digital systems [28], [29], [35]. In this approach, a generic beatnote signal with nominal frequency f_b, sampled by the ADC at times n/f_s, n integer, is described as a discrete voltage

$$V[n] = A[n]\sin(2\pi f_b n/f_s + \varphi[n]) \tag{4}$$

where $A[n]$ and $\varphi[n]$ indicate amplitude and phase at each sampling interval. This signal is mixed with two numerically generated references at the same nominal frequency f_b, but having $\pi/2$ relative phase shift

$$\begin{aligned} i[n] &= \cos(2\pi f_b n/f_s) \\ q[n] &= \sin(2\pi f_b n/f_s). \end{aligned} \tag{5}$$

In our implementation, $i[n]$ and $q[n]$ are generated using Xilinx DDS cores; the frequency resolution is set to 48 bits—the highest possible—to minimize frequency errors, while 16 bit output data width has been chosen as a good compromise between rounding noise and computational complexity. All the numerical oscillators of this section are run-time programmable to simplify the laser locking setup phase.

Mixed signals are low-pass filtered using finite-impulse-response (FIR) filters. Their output is a weighted sum of $N+1$ terms, where the filter order is defined by N, and the frequency response by weight coefficients h. We used $N = 71$ with bandwidth 2.5 MHz. The obtained signals consist in the in-phase and quadrature components

$$\begin{aligned} I[n] &= \sum_{m=0}^{N-1} h[m]i[n-m]V[n-m] = \frac{1}{2}A[n]\cos(\varphi[n]) \\ Q[n] &= \sum_{m=0}^{N-1} h[m]q[n-m]V[n-m] = \frac{1}{2}A[n]\sin(\varphi[n]). \end{aligned} \tag{6}$$

The two are finally combined to retrieve the instantaneous amplitude and phase of the signal

$$\begin{aligned} A[n] &= 2\sqrt{I[n]^2 + Q[n]^2} \\ \varphi'[n] &= \arctan(Q[n], I[n]). \end{aligned} \tag{7}$$

Note that $\varphi'[n]$ is a wrapped version of $\varphi[n]$, as the domain of the inverse tangent function is defined between $-\pi/2$ and $+\pi/2$ only. $\varphi[n]$ is obtained from $\varphi'[n]$ by removing discontinuities larger than π via a suitable unwrap algorithm.

The block diagram of the digital processing for each of the input channels is summarized in Fig. 1(a).

D. Error Signal Generation

The phases of each beatnote $\varphi_{b,m}$, $\varphi_{b,s}$, and φ_0 are obtained by I/Q demodulation as described by (5)–(7) running on three parallel channels. The three are combined according to the formula

$$\varphi_{\text{err}} = k\left(N_s\varphi_{b,m} + N_s'\varphi_0 + N_m\varphi_{b,s} + N_m'\varphi_0\right) \tag{8}$$

which is a different formulation of (3) in which the division by N_s has been removed to minimize latency (otherwise in a range of tens of clock cycles) and precision loss introduced by the Divide core. Also, independent scaling coefficients were made explicit for each raw phase to keep into account the correct sign for beatnotes at $f_{b,m}$, $f_{b,s}$, and f_0. Therefore, $|N_m| = |N_m'|$, but their sign may differ, and similarly for N_s. An additional scaling factor k is considered to match the DAC output range to which φ_{err} is subsequently sent and tune the PID overall gain.

In our implementation, scaling by k has been implemented as a simple shift to keep complexity low, while rounding is only performed as the last step. For locking additional lasers, it is enough to configure further ADC channels—one for each laser—and update scaling coefficients, while channels related to the comb offset frequency and reference laser are common to all pairs. This enables to lock up to six independent lasers using the provided eight-channel ADC and DAC boards. The block diagram of the processing chain is shown in Fig. 1(b) together with coefficient sets that fulfill (8) for each laser pair.

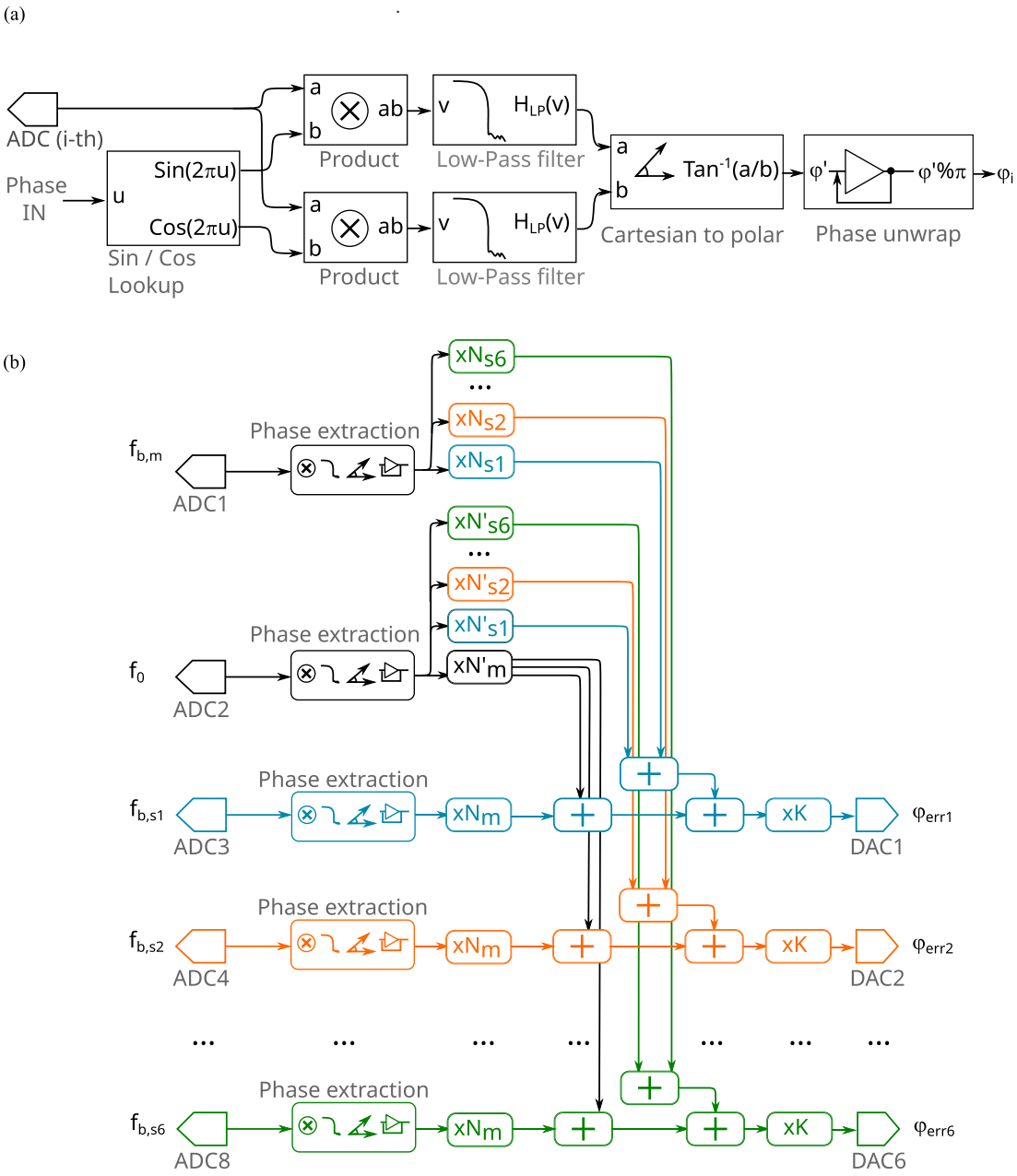

Fig. 1. (a) Digital signal processing of the ith input channel performed by the FPGA. u, a, b, and v represent arbitrary input signals. The "Phase IN" input is obtained at each iteration by multiplying the discrete time by the nominal frequency of the given beatnote. (b) Block diagram showing the combination of sampled phases to obtain the error signals $\varphi_{\text{err1}}, \ldots, \varphi_{\text{err6}}$ used for locking S1, . . . , S6 to the main (M). Blue, orange, and green coloring indicate blocks that are related to S1, S2, and S6. Two-inputs/one-output sum boxes reflect the structure of FPGA blocks.

E. Output Stage

φ_{err} can be sent to the DAC as it is and used to feed an external PID control loop to stabilize the secondary laser to the main. This solution is feasible whenever the FPGA board and the secondary laser are placed within a few meters, so that the analog correction signal can be sent to the latter via coaxial cable. However, in many cases, the two are in different laboratories. In those cases, transferring a RF instead of a dc signal is preferable, as it is more immune to interference, attenuation, and ground loops. To this purpose, we designed the output stage as a 48-bit DDS producing a sine-wave whose frequency is continuously adjusted to be $f_{\text{out}} = f_{\text{nom}} + c\varphi_{\text{err}}$, i.e., it deviates from a preset nominal value f_{nom} by a small quantity proportional to φ_{err} via a coefficient c. At any clock cycle, when a new estimation of φ_{err} becomes available, the increment from the previous value is computed. Scaling by c is implemented as a shift to keep complexity low, and the DDS frequency is adjusted by updating the corresponding tuning word. We conveniently chose $f_{\text{nom}} = 10$ MHz, as it is easily demodulated at the destination laboratory exploiting the 10 MHz reference signal which is usually available.

F. Latencies

Each of the above operations contributes to the overall processing latency, which is a critical parameter as it sets

the ultimate servo bandwidth. Here, we summarize the main contribution of individual steps. The latency introduced by I/Q demodulation, filtering, and unwrapping is about 90 clock cycles, corresponding to 360 ns at a 250 MHz sampling rate. Of those, three clock cycles are contributed by multiplication of the sampled signal with i and q references, 36 by the 71-tap low-pass filter, about 36 by the arctan computation and about 15 by the unwrap. The implementation of (8) contributes 21 clock cycles, or 84 ns. Finally, the digital delay for encoding the phase error into a RF tone at the output stage is 44 clock cycles, or 176 ns. Analog/digital conversion contributes additional latencies that cannot be a priori calculated. We measured them by connecting internally ADCs and DACs and measuring the delay with which an analog square wave is sampled and reproduced at the output. Altogether, analog/digital and digital/analog conversion contribute an additional delay of 274 ns, on top of the above. Overall, the total latency of digital processing amounts to 718 and 894 ns in the phase-error or frequency output mode, respectively.

III. FPGA Residual Noise

A. Experimental Setup

We used the FPGA board to simultaneously phase-lock a pair of lasers (S1 and S2) in the telecom region around 1542 nm to a main reference laser (M) at 1156 nm. For this purpose, we configured the FPGA board with four ADC channels, dedicated to processing beatnotes at $f_{b,m}$, $f_{b,s1}$, $f_{b,s2}$, and f_0. The other four channels were not used in this demonstration, but can be configured to lock additional lasers. We assigned a nominal frequency to each channel, arbitrarily chosen within about 100 kHz from the actual beatnote frequency; i and q were synthetized accordingly.

Two different sets of coefficients were set, according to the implementation of (8) for each laser pair and with sign depending on the beatnotes sign [see Fig. 1(b)]. The two error signals (φ_{err1} and φ_{err2}) were routed to two independent DAC channels and integrated by analog, external control loops PID1 and PID2, feeding back on the two lasers. A comprehensive telemetry section has been implemented to assess the algorithm behavior during validation: raw ADC samples or processed datasets can be saved to embedded memories and readily analyzed or displayed using Jupyter notebooks. Phase samples for individual channels as well as φ_{err} can be decimated and saved either to an embedded or a first-in first-out (FIFO) memory for long-term data analysis.

To characterize the FPGA board residual noise, we also set-up a hardware chain, configured to generate a transfer beatnote at a time either between M and S1, or between M and S2, or between S1 and S2. The RF signals corresponding to the three beatnotes were detected with about 85 dB SNR in 1 Hz bandwidth, bandpass filtered and split into two parts each, one directed to the FPGA processing chain, the rest to the hardware synthesis chain. In this branch, RF signals were up-shifted to match available bandpass filters, amplified, and mixed with f_0, then used to clock a pair of 48-bit DDSs (AD9912 by Analog Devices) [26]. The DDSs were configured to implement scaling coefficients of $1/4$ on the M arm and $N_m/N_{s1}/4$, or $N_m/N_{s2}/4$, or $N_{s2}/N_{s1}/4$ on the S1 and S2 arm, that satisfied (3) in the three cases; global scaling by $1/4$ was necessary to fulfill Nyquist criterion in the employed DDSs. By measuring the hardware transfer beatnote residual noise, we quantified the upper limit to the phase-locked loops noise contributed by the FPGA alone. Phase fluctuations arising in the optical components of the comb (e.g., fiber delivery systems or noncommon optical paths) are excluded from this analysis as they are common to both the analog and the digital synthesis chain. The test-setup is sketched in Fig. 2.

Focusing on the optical equipment, M is a tapered amplifier diode laser (DLC TA PRO by Toptica) at 1156 nm (259 THz), stabilized to a high-finesse Fabry–Perot cavity with a flicker-floor instability of about 1×10^{-15} and used to interrogate INRIM Yb optical lattice clock IT-Yb1 [43]. S1 is a 1542.14 nm (194.400 THz) external cavity diode laser in butterfly package (PLANEX by Redfern Integrated Optics) with an instantaneous linewidth <10 kHz; we chose this device as it is often used in many laboratories for fiber-based frequency distribution and remote atomic clock comparison [2]. S2 is a continuously tunable diode laser (CTL-1500 by Toptica) operated at 1543.51 nm (194.228 THz) with a free-space cavity and linewidth <100 kHz. The comb is a self-referenced Er-doped fiber comb whose repetition rate, 250 MHz, is locked to one of INRIM H-masers. The comb modes in the 1550 nm region have a linewidth of about 150 kHz. Comb radiation spanning between the employed lasers was extracted from a supercontinuum port covering the 1–2 μm spectrum. This is obtained by amplifying the native comb spectrum in the 1550 nm region with an Erbium-doped fiber amplifier (EDFA) and broadening it into a highly nonlinear fiber (HNLF). The optical spectrum of the used comb, together with that of the cw lasers, is shown in [42]. Part of the comb output is independently amplified, frequency-duplicated into a periodically poled Lithium Niobate crystal and sent to an $f-2f$ interferometer for offset-frequency stabilization. The supercontinuum output is dispersed on a grating after being combined with the three cw lasers. We detected the beatnotes of S1 and S2 with the comb on the same photodiode at frequencies $f_{b,s1}$ and $f_{b,s2}$, while the beatnote between M and the comb at frequency $f_{b,m}$ was collected at a different angle and measured on a separate photodiode.

B. Results

Fig. 3 summarizes the results of this characterization. The blue and orange curves show the phase noise of free-running beatnotes between the comb and S1, or S2. In the case of S1 (blue), the noise is dominated by the comb tooth, specifically by the H-maser referencing f_{rep}. A similar result, not shown here for clarity, was obtained by measuring the beatnote between the free-running M laser and the comb. In the case of S2 (orange), the noise at Fourier frequencies lower than 1 kHz is dominated by the intrinsic noise of S2. When S1 and S2 are locked to M via the FPGA, the comb noise is rejected according to the transfer oscillator principle and the lasers noise is canceled within a bandwidth of $\approx$200 kHz. The green (red) curves show the noise of the hardware transfer

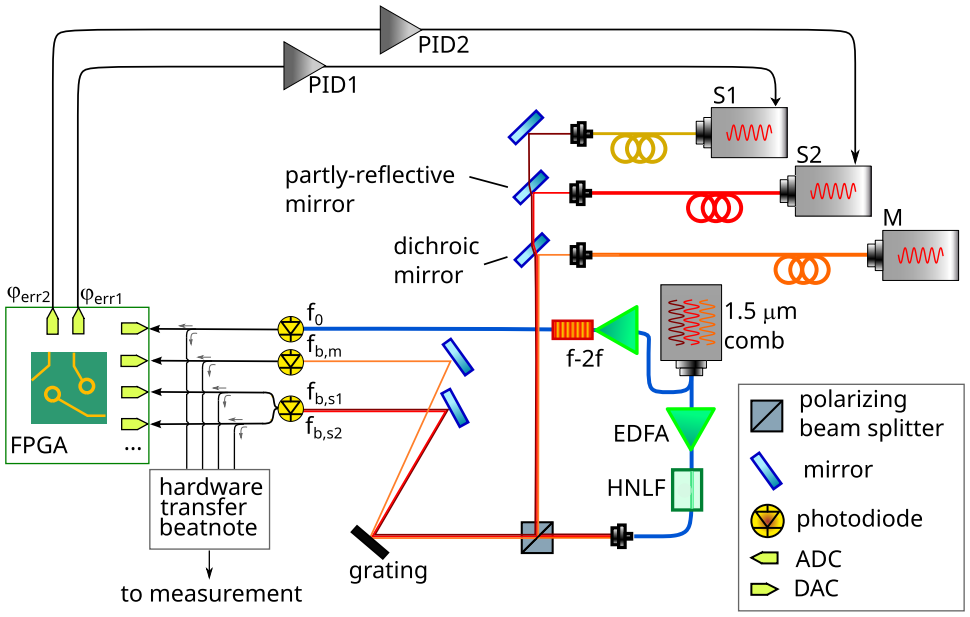

Fig. 2. Experimental setup used to characterize the digital synthesis chain. The FPGA synthetizes an error signal for locking S1 and S2 to a common laser (M), while a hardware transfer beatnote is produced with analog components and measured to provide an out-of-loop characterization of the electronics. EDFA: Erbium-doped fiber amplifier; HNLF.

beatnote between S1(S2) and M in this condition. The noise of the transfer beatnote between S1 and S2 exhibits a similar behavior and is not shown here for clarity. The locking bandwidth is limited by the loop latency, which we measured to be 1.35 μs. This is higher than expected from the FPGA alone (about 718 ns). Such a discrepancy could be due to underestimated latencies in the oversampling/undersampling logic present in the FPGA internal ADCs and DACs, or group delays of analog components. In all cases, the residual noise is $<1 \times 10^{-4}$ rad^2/Hz until 10 mHz, indicating effective suppression of the lasers and comb noise, irrespective of the noise level of the original beatnotes, and a very low contribution by the FPGA.

Interestingly, the residual noise shows a peculiar structure in the Fourier spectrum between 5 Hz and 100 kHz, which we explained in terms of a delay mismatch between the electronic paths carrying the signals at $f_{b,m}$ and $f_{b,s1}$ or $f_{b,s2}$ in the hardware beatnote synthesis chain, mostly due to analog RF bandpass filters. A noncommon delay δ between the two detection chains limits the suppression of the comb's tooth noise to a factor $(2\pi f\delta)^2$. The noise expected from $\delta \approx 500$ ns is shown as the gray shaded area and is consistent with the filters we used in the lock of S1 to M, well explaining the observed results. This kind of effect is often over-looked when implementing hardware-based transfer beatnotes; while its impact is in most cases negligible at low Fourier frequencies (e.g., 1 Hz and below), it may become a concern for applications requiring ultrahigh spectral purity at kHz frequencies and above, or in cases where the RF signal referencing f_{rep} is noisy. Digital systems mitigate this effect, thanks to a drastic reduction of analog components that are more subject to uncontrolled delays and delay-variations over time. At the same time, they enable a better control of the filtering bandwidth, improving the SNR.

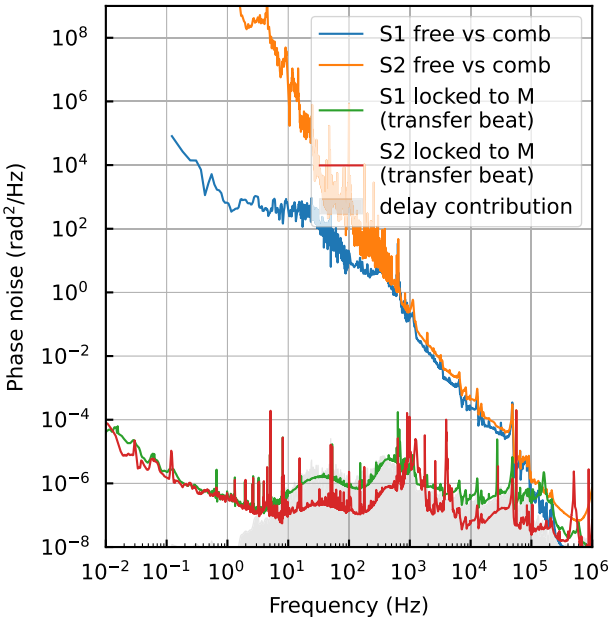

Fig. 3. Blue: noise of the beatnote between free-running S1 and the comb, mostly limited by the comb. Orange: noise of the beatnote between free-running S2 and the comb, showing noise excess of S2 below 1 kHz. Green (red): noise of the hardware transfer beatnote between S1 (S2) and M when S1 (S2) is locked to M via the FPGA board. Gray shadowed area: estimated unsuppressed noise of f_{rep} due to a 500 ns mismatch in the electronics paths in the hardware synthesis chain. All curves are referred to the spectral region of S1 and S2.

IV. Frequency-Stability Transfer Across the Spectrum

A. Experimental Setup

As a showcase application, we used the optical comb and our developed FPGA board to transfer the spectral properties of our Yb clock laser at 1156 nm to radiation

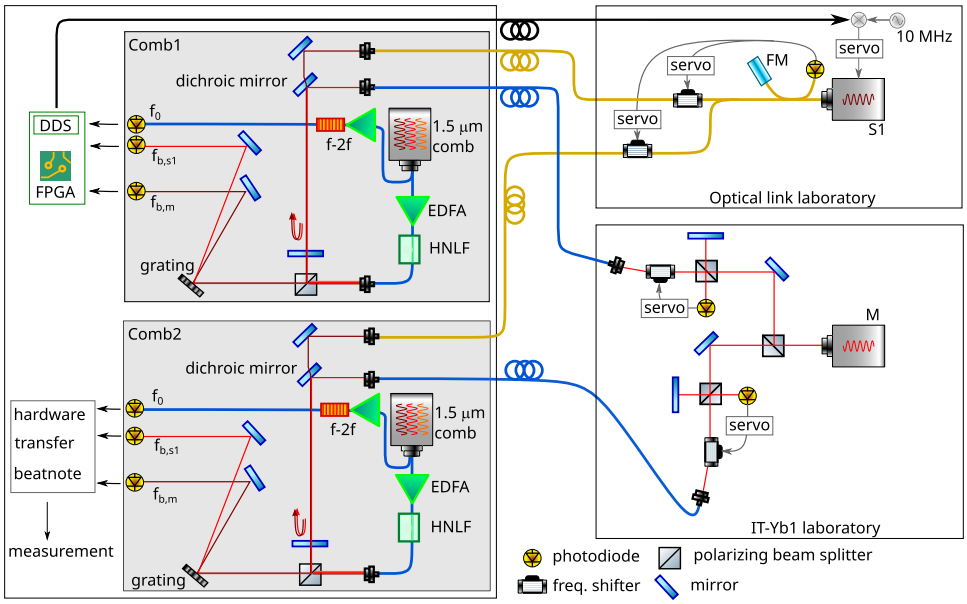

Fig. 4. Experimental scheme used to characterize the spectral transfer between 1156 and 1542 nm. The two lasers and the combs are housed in different laboratories of the INRIM campus. Radiation at 1156 nm is delivered to the combs using polarization-maintaining fibers; radiation at 1542 nm is delivered to the combs using single-mode fibers. Comb1 and the FPGA board are used to lock S1, housed in the optical link laboratory at INRIM, to M, which is the clock laser of INRIM Yb lattice clock IT-Yb1, housed in the Yb optical clock laboratory. The distance between the optical link laboratory and the comb is about 130 m. DDS: direct digital synthesizer; EDFA: Erbium-doped fiber amplifier; HNLF; FM: Faraday-rotator mirror.

at 1542 nm that is disseminated to remote laboratories via stabilized fibers along the Italian Quantum Backbone [44]. We used M and S1 as the main and secondary lasers, respectively, and the experimental setup is similar to the one introduced in Section III-A. However, in this showcase, the lasers and comb were housed in three different laboratories of the INRIM campus, connected by 132 m-long coaxial cables and phase-stabilized optical fibers. Thus, we configured the FPGA board to encode the error signal as a frequency deviation from a 10 MHz tone. This RF signal is sent to the laboratory where S1 is housed and here demodulated to phase-lock it.

To evaluate the overall performances of this setup, we sent part of each laser beam to an independent optical comb, produced their transfer beatnote with a hardware synthesis chain, and measured its noise. This scheme enabled us to quantify the residual noise of the spectral transfer process in a comprehensive manner, including contributions from the comb, fiber-delivery systems, noncommon optical paths and realistic propagation delays. The experimental scheme is sketched in Fig. 4. S1 is split into two arms and sent to the two combs (Comb1 and Comb2) via phase-stabilized optical fibers, with about 100 μW of optical power reaching the two. The fiber phase-stabilization scheme [45] is based on two Michelson interferometers designed as in [27]. The two share a common reference mirror (Faraday mirror FM), while the remote reflector is a partially transmitting mirror on the comb optical bench, free-space mounted and shared with the M laser's path. The round-trip signal on each of the two paths is combined with the reference light on the same photodiode. In addition to being used as actuators, frequency shifters are set such that the two beatnotes differ by 22 MHz and can be spectrally separated to independently stabilize the two links. Delivery of radiation at 1156 nm is similar to that of S1, except for the fact that two separate reference mirrors are used for the two links and, the path being shorter, polarization maintaining fibers are used [46]. About 1 mW of optical power reaches the two combs. The two combs are identical Er: fiber combs but we stabilized them in different manners to avoid any common-mode suppression of their repetition rate noise, undesired during the characterization phase. Comb1 is operated in the narrow-linewidth regime, i.e., we detect and stabilize the beatnote between the 1156 nm laser and the closest comb tooth, feeding back onto the repetition rate with a bandwidth of 300 kHz. The repetition rate of Comb2 is stabilized directly onto a H-maser with a bandwidth of 250 Hz. On both combs, radiation at 1156 nm and 1542 nm is extracted from the amplified supercontinuum output and combined with the two cw lasers on a polarization beam-splitter positioned about 1 cm after the common retro-reflecting mirror. The three overlapped beams are dispersed by a grating and sent to two photodiodes for beatnotes detection. With this scheme, beatnotes are insensitive to air density fluctuations in most of the free-space paths, as they are common between the comb and the lasers beam.

The phase noise and instability of the hardware transfer beatnote generated on Comb2 were characterized with different instruments: first, with a phase noise analyzer (PNA) (5125 by Microsemi) whose sampling rate and measurement bandwidth can be arbitrarily set to reject aliasing noise [47]. This is critical when aiming to measure optical signals featuring high phase noise at Fourier frequencies in the kHz range. Second, for long-term measurements, we counted the hardware transfer beatnote on a dead-time-free frequency

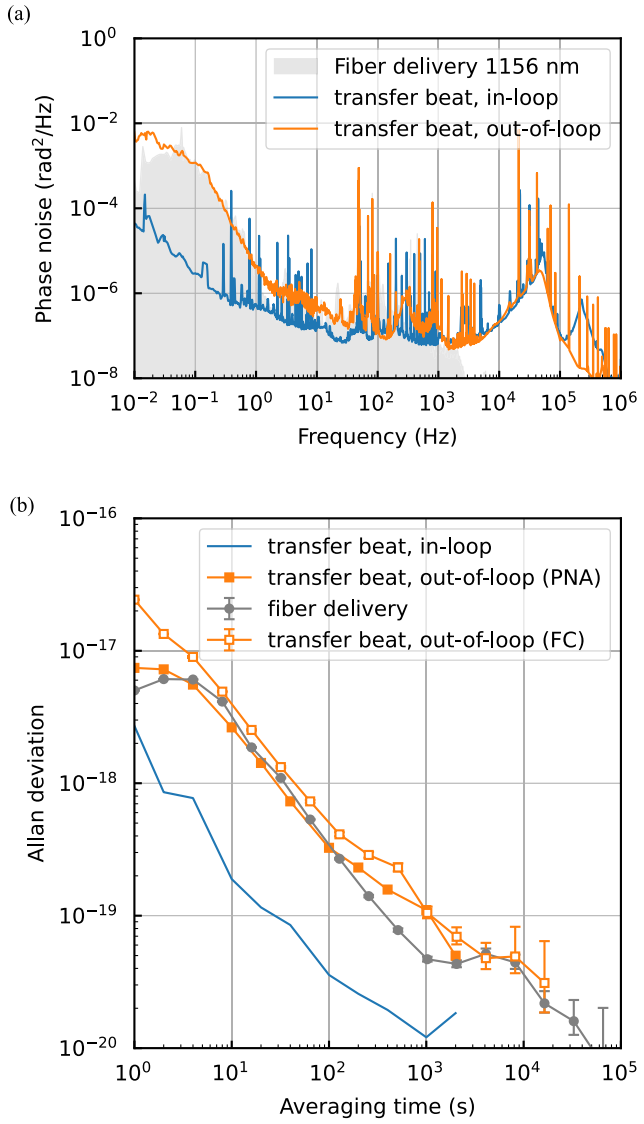

Fig. 5. (a) Orange curve: phase noise of the spectral transfer between a 1156 and a 1542 nm laser, measured by producing a hardware transfer beatnote on a separate comb. Blue curve: noise contributed by the FPGA synthesis chain, measured as described in Section III-A. Shadowed area: noise of the fiber delivery systems. (b) Blue curve: instability contribution of the FPGA board alone. Gray line with circles: instability of the fiber delivery systems. Orange curve with filled squares: instability of the out-of-loop beatnote measured with an aliasing-free PNA, on a 0.5 Hz measurement bandwidth. Orange curve with empty squares: instability of the out-of-loop beatnote measured with a dead-time-free FC in averaging mode, with intrinsic sampling rate of 1 kHz and report time of 1 s.

counter (FC), set to averaging mode and with 1 s reporting interval.

B. Results

Fig. 5(a) shows the noise power spectral density of the transfer beatnote measured on Comb2 (orange) together with the in-loop transfer beatnote, measured on Comb1 as described in Section III-A (blue) and representing the upper limit to the FPGA and hardware chain noise floor. The plot also shows the noise contributed by the fiber delivery system of the 1156 nm laser (shadowed gray area), that represents the major limit to the stability transfer at Fourier frequencies <1 kHz. The residual noise of the digital electronics only emerges at Fourier frequencies higher than 10 kHz; at those frequencies, the noise suppression is limited by the large propagation delay of the optical beam and the return correction signal (1.32 μs), combined with the measured processing latency (1.35 μs for the phase extraction and 176 ns for driving the DDS output stage) and the presence of a low-pass filter with 400 ns group delay at the 10 MHz demodulation stage. The corresponding frequency instabilities are shown in Fig. 5(b): the contribution of the FPGA (blue) is 3×10^{-18} at 1 s, and that of the 1156 nm fiber delivery (gray, circles) is 6×10^{-18} at 1 s. The out-of-loop transfer beatnote derived from Comb2 (orange, filled squares) and obtained from the PNA is mostly limited by the latter effect, and shows a 1 s instability of 8×10^{-18}.

The long-term instability, calculated from FC data (orange curve, empty squares), is consistent with that obtained by the PNA and extends in duration, achieving the low 10^{-20} region after day-long integration. Frequency ratios measured on the two combs show no resolved discrepancy, confirming the absence of frequency biases. The short-term instability derived from the FC is increased with respect to the PNA due to aliasing from the transfer-beatnote phase noise at Fourier components above the counter sampling rate (1 kHz), and due to a difference in the effective measurement bandwidth of the two instruments [47].

Overall, the obtained spectral transfer is demonstrated to contribute an instability that is negligible with respect to the best ultrastable lasers available today.

V. Discussion and Conclusion

We developed an FPGA-based electronics chain capable of synthesizing the transfer beatnote between a common reference laser with superior stability and multiple independent lasers in different spectral domains simultaneously, even with the comb locked in the RF-domain that causes broader teeth linewidths and higher beatnote noise. Spectral conversion between 1156 and 1542 nm is demonstrated with 8×10^{-18} instability at 1 s, limited by the optical components of the setup, specifically the fiber-based delivery systems, while the contribution of the FPGA board alone is 3×10^{-18} at 1 s. Digital implementation is effective in reducing the amount of bulk devices and hence the complexity of the system and related undesired effects, such as latency of analog components or long-term thermal drifts. Our multilaser locking platform is organized with a modular approach that enables straightforward reconfiguration and allocation of up to six independent locking paths. This number is limited by available ADC and DAC channels of our board, which is eight. The utilization of logic resources recorded with four operating channels was minimal, supporting the inclusion of four additional measurement paths. This system enables to take full advantage of the optical comb as a transfer oscillator, allowing the transfer of the reference laser spectral properties to any region covered by the comb spectrum, serving thus a potentially high number of independent experiments simultaneously. This feature is especially useful in laboratories maintaining an ensemble of optical clocks that could thus be

probed with a single clock laser, to reject quantum projection noise and assess complex interrogation schemes. For this application, Er-doped fiber combs are particularly suited, featuring a broadband-spanning optical spectrum covering the 1–2 μm band [42] and the regions of interest for many optical clock species, e.g., Sr (clock wavelength 1396 nm/2), Sr^+ (clock wavelength 1348 nm/2), Ca (clock wavelength 1314 nm/2), and Hg^+ (clock wavelength 1126 nm/4), [48]. While the choice of wavelengths in our demonstration was motivated by a concrete need, i.e., to convert the properties of our Yb clock laser at 1156 nm to the wavelength region of fiber-based frequency dissemination at 1542 nm, results can be considered representative also for other target wavelengths. The possibility to reach the 1550 nm region also suggests perspectives for exploitation in distributed clocks networks, connected by phase-stabilized fiber links [18], [21]. Spectral extension to different bandwidths is also possible, although the implementation of single-branch topologies may be difficult [27], while multibranch topologies could introduce instability from noncommon paths [26].

Thanks to its digital nature, the present scheme can also be upgraded to perform more complex tasks, e.g., implement gated detection to increase immunity to SNR drops, include alarms and automated switches to different locking schemes in case one of the lasers becomes unavailable, or implement interbranch stabilization by simultaneously sampling a single signal on different comb branches [49], [50]. Furthermore, the possibility to log raw data enables real-time performance monitoring without aliasing or resolution limitations often encountered with FCs. This feature could also be exploited in open loop conditions where the board operates just as a multichannel phase meter, provided that the phase increments are output instead of pure phase, to avoid saturation in the logic in case of long-term measurements.

Datasets underlying plots for this publication are available at [51].

REFERENCES

[1] P. Kwee et al., "Stabilized high-power laser system for the gravitational wave detector advanced LIGO," *Opt. Exp.*, vol. 20, no. 10, pp. 10617–10634, May 2012. [Online]. Available: https://opg.optica.org/oe/abstract.cfm?URI=oe-20-10-10617

[2] C. Clivati et al., "Coherent optical-fiber link across Italy and France," *Phys. Rev. Appl.*, vol. 18, no. 5, Nov. 2022, Art. no. 054009, doi: 10.1103/PhysRevApplied.18.054009.

[3] L. F. Livi et al., "Synthetic dimensions and spin-orbit coupling with an optical clock transition," *Phys. Rev. Lett.*, vol. 117, no. 22, Nov. 2016, Art. no. 220401, doi: 10.1103/PhysRevLett.117.220401.

[4] E. Oelker et al., "Demonstration of 4.8×10^{-17} stability at 1 s for two independent optical clocks," *Nature Photon.*, vol. 13, no. 10, pp. 714–719, Oct. 2019.

[5] K. Beloy et al., "Frequency ratio measurements at 18-digit accuracy using an optical clock network," *Nature*, vol. 591, no. 7851, pp. 564–569, Mar. 2021.

[6] J. Yao et al., "Optical-clock-bsed time scale," *Phys. Rev. Appl.*, vol. 12, no. 4, Oct. 2019, Art. no. 044069, doi: 10.1103/PhysRevApplied.12.044069.

[7] W. R. Milner et al., "Demonstration of a timescale based on a stable optical carrier," *Phys. Rev. Lett.*, vol. 123, no. 17, Oct. 2019, Art. no. 173201, doi: 10.1103/PhysRevLett.123.173201.

[8] V. Formichella et al., "Year-long optical time scale with sub-nanosecond capabilities," *Optica*, vol. 11, no. 4, pp. 523–530, Apr. 2024. [Online]. Available: https://opg.optica.org/optica/abstract.cfm?URI=optica-11-4-523

[9] T. Kobayashi et al., "Generation of a precise time scale assisted by a near-continuously operating optical lattice clock," *Phys. Rev. Appl.*, vol. 21, no. 6, Jun. 2024, Art. no. 064015. [Online]. Available: https://link.aps.org/doi/10.1103/PhysRevApplied.21.064015

[10] N. Dimarcq et al., "Roadmap towards the redefinition of the second," *Metrologia*, vol. 61, no. 1, Dec. 2023, Art. no. 012001.

[11] F. Riehle, P. Gill, F. Arias, and L. Robertsson, "The CIPM list of recommended frequency standard values: Guidelines and procedures," *Metrologia*, vol. 55, no. 2, pp. 188–200, Feb. 2018, doi: 10.1088/1681-7575/aaa302.

[12] C. Lisdat et al., "A clock network for geodesy and fundamental science," *Nature Commun.*, vol. 7, p. 12443, Aug. 2016, doi: 10.1038/ncomms12443.

[13] J. Grotti et al., "Geodesy and metrology with a transportable optical clock," *Nature Phys.*, vol. 14, no. 5, pp. 437–441, May 2018, doi: 10.1038/s41567-017-0042-3.

[14] M. Takamoto et al., "Test of general relativity by a pair of transportable optical lattice clocks," *Nature Photon.*, vol. 14, no. 7, pp. 411–415, Jul. 2020.

[15] W. F. McGrew et al., "Atomic clock performance enabling geodesy below the centimetre level," *Nature*, vol. 564, no. 7734, pp. 87–90, Dec. 2018.

[16] R. M. Godun et al., "Frequency ratio of two optical clock transitions in $^{171}Yb^+$ and constraints on the time variation of fundamental constants," *Phys. Rev. Lett.*, vol. 113, no. 21, Nov. 2014, Art. no. 210801. [Online]. Available: https://link.aps.org/doi/10.1103/PhysRevLett.113.210801

[17] N. Huntemann, B. Lipphardt, C. Tamm, V. Gerginov, S. Weyers, and E. Peik, "Improved limit on a temporal variation of m_p/m_e from comparisons of Yb^+ and Cs atomic clocks," *Phys. Rev. Lett.*, vol. 113, no. 21, Nov. 2014, Art. no. 210802. [Online]. Available: https://link.aps.org/doi/10.1103/PhysRevLett.113.210802

[18] G. Barontini et al., "Measuring the stability of fundamental constants with a network of clocks," *EPJ Quantum Technol.*, vol. 9, no. 1, p. 12, 2022.

[19] D. Kedar et al., "Frequency stability of cryogenic silicon cavities with semiconductor crystalline coatings," *Optica*, vol. 10, no. 4, pp. 464–470, Apr. 2023. [Online]. Available: https://opg.optica.org/optica/abstract.cfm?URI=optica-10-4-464

[20] J. M. Robinson et al., "Thermal noise and mechanical loss of SiO_2/Ta_2O_5 optical coatings at cryogenic temperatures," *Opt. Lett.*, vol. 46, no. 3, pp. 592–595, Feb. 2021. [Online]. Available: https://opg.optica.org/ol/abstract.cfm?URI=ol-46-3-592

[21] M. Schioppo et al., "Comparing ultrastable lasers at 7×10^{-17} fractional frequency instability through a 2220 km optical fibre network," *Nature Commun.*, vol. 13, no. 1, p. 212, Jan. 2022.

[22] S. A. Diddams, K. Vahala, and T. Udem, "Optical frequency combs: Coherently uniting the electromagnetic spectrum," *Science*, vol. 369, no. 6501, Jul. 2020, Art. no. eaay3676, doi: 10.1126/science.aay3676.

[23] D. Nicolodi, B. Argence, W. Zhang, R. Le Targat, G. Santarelli, and Y. Le Coq, "Spectral purity transfer between optical wavelengths at the 10^{-18} level," *Nature Photon.*, vol. 8, no. 3, pp. 219–223, Mar. 2014.

[24] H. R. Telle, B. Lipphardt, and J. Stenger, "Kerr-lens, mode-locked lasers as transfer oscillators for optical frequency measurements," *Appl. Phys. B: Lasers Opt.*, vol. 74, no. 1, pp. 1–6, Jan. 2002.

[25] L. A. M. Johnson, P. Gill, and H. S. Margolis, "Evaluating the performance of the NPL femtosecond frequency combs: Agreement at the 10^{-21} level," *Metrologia*, vol. 52, no. 1, pp. 62–71, Jan. 2015, doi: 10.1088/0026-1394/52/1/62.

[26] P. Barbieri, C. Clivati, M. Pizzocaro, F. Levi, and D. Calonico, "Spectral purity transfer with 5×10^{-17} instability at 1 s using a multibranch Er: Fiber frequency comb," *Metrologia*, vol. 56, no. 4, Jul. 2019, Art. no. 045008, doi: 10.1088/1681-7575/ab2b0f.

[27] E. Benkler, B. Lipphardt, T. Puppe, R. Wilk, F. Rohde, and U. Sterr, "End-to-end topology for fiber comb based optical frequency transfer at the 10^-21 level," *Opt. Exp.*, vol. 27, no. 25, pp. 36886–36902, Dec. 2019. [Online]. Available: https://opg.optica.org/oe/abstract.cfm?URI=oe-27-25-36886

[28] A. Tourigny-Plante, V. Michaud-Belleau, N. B. Hébert, H. Bergeron, J. Genest, and J.-D. Deschĕnes, "An open and flexible digital phase-locked loop for optical metrology," *Rev. Sci. Instrum.*, vol. 89, no. 9, Sep. 2018, Art. no. 093103.

[29] J. A. Sherman and R. Jördens, "Oscillator metrology with software defined radio," *Rev. Sci. Instrum.*, vol. 87, no. 5, May 2016, Art. no. 054711, doi: 10.1063/1.4950898.

[30] C. E. Calosso, F. Vernotte, V. Giordano, C. Fluhr, B. Dubois, and E. Rubiola, "Frequency stability measurement of cryogenic sapphire oscillators with a multichannel tracking DDS and the two-sample covariance," *IEEE Trans. Ultrason., Ferroelectr., Freq. Control*, vol. 66, no. 3, pp. 616–623, Mar. 2019.

[31] C. E. Calosso et al., "Doppler-stabilized fiber link with 6 dB noise improvement below the classical limit," *Opt. Lett.*, vol. 40, no. 2, pp. 131–134, Jan. 2015. [Online]. Available: https://opg.optica.org/ol/abstract.cfm?URI=ol-40-2-131

[32] S. Mukherjee et al., "Digital Doppler-cancellation servo for ultrastable optical frequency dissemination over fiber," *IEEE Trans. Ultrason., Ferroelectr., Freq. Control*, vol. 69, no. 2, pp. 878–885, Feb. 2022.

[33] M. Matusko et al., "Fully digital platform for local ultra-stable optical frequency distribution," *Rev. Sci. Instrum.*, vol. 94, no. 3, Mar. 2023, Art. no. 034716, doi: 10.1063/5.0138599.

[34] S. Herbers, S. Dörscher, E. Benkler, and C. Lisdat, "Phase noise of frequency doublers in optical clock lasers," *Opt. Exp.*, vol. 27, no. 16, pp. 23262–23273, Aug. 2019.

[35] S. Donadello, E. K. Bertacco, D. Calonico, and C. Clivati, "Embedded digital phase noise analyzer for optical frequency metrology," *IEEE Trans. Instrum. Meas.*, vol. 72, pp. 1–12, 2023.

[36] L. C. Sinclair et al., "Invited article: A compact optically coherent fiber frequency comb," *Rev. Sci. Instrum.*, vol. 86, no. 8, Aug. 2015, Art. no. 081301, doi: 10.1063/1.4928163.

[37] E. D. Caldwell, L. C. Sinclair, N. R. Newbury, and J.-D. Deschenes, "The time-programmable frequency comb and its use in quantum-limited ranging," *Nature*, vol. 610, no. 7933, pp. 667–673, Oct. 2022.

[38] J. K. Shaw, C. Fredrick, and S. A. Diddams, "Versatile digital approach to laser frequency comb stabilization," *OSA Continuum*, vol. 2, no. 11, pp. 3262–3271, Nov. 2019. [Online]. Available: https://opg.optica.org/osac/abstract.cfm?URI=osac-2-11-3262

[39] M. Takamoto, T. Takano, and H. Katori, "Frequency comparison of optical lattice clocks beyond the dick limit," *Nature Photon.*, vol. 5, no. 5, pp. 288–292, May 2011.

[40] L. Zhou, J. Lin, Y. Jing, and Z. Yuan, "Twin-field quantum key distribution without optical frequency dissemination," *Nat. Commun.*, vol. 14, no. 1, p. 928, Feb. 2023.

[41] *Nextlasers_FPGA*. Accessed: Jan. 11, 2025. [Online]. Available: Https://gitlab.linksfoundation.com/psavio/nextlasers_fpga

[42] M. Risaro, P. Savio, M. Pizzocaro, F. Levi, D. Calonico, and C. Clivati, "Improving the resolution of comb-based frequency measurements using a track-and-hold amplifier," *Phys. Rev. Appl.*, vol. 18, no. 6, Dec. 2022, Art. no. 064010. [Online]. Available: https://link.aps.org/doi/10.1103/PhysRevApplied.18.064010

[43] I. Goti et al., "Absolute frequency measurement of a Yb optical clock at the limit of the Cs fountain," *Metrologia*, vol. 60, no. 3, May 2023, Art. no. 035002, doi: 10.1088/1681-7575/accbc5.

[44] C. Clivati et al., "Robust optical frequency dissemination with a dual-polarization coherent receiver," *Opt. Exp.*, vol. 28, no. 6, pp. 8494–8511, Mar. 2020. [Online]. Available: https://opg.optica.org/oe/abstract.cfm?URI=oe-28-6-8494

[45] P. A. Williams, W. C. Swann, and N. R. Newbury, "High-stability transfer of an optical frequency over long fiber-optic links," *J. Opt. Soc. Amer. B, Opt. Phys.*, vol. 125, no. 8, pp. 1284–1293, Jul. 2008. [Online]. Available: https://opg.optica.org/josab/abstract.cfm?URI=josab-25-8-1284

[46] B. Rauf, M. C. Vélez López, P. Thoumany, M. Pizzocaro, and D. Calonico, "Phase noise cancellation in polarisation-maintaining fibre links," *Rev. Sci. Instrum.*, vol. 89, no. 3, Mar. 2018, Art. no. 033103.

[47] C. E. Calosso, C. Clivati, and S. Micalizio, "Avoiding aliasing in Allan variance: An application to fiber link data analysis," *IEEE Trans. Ultrason., Ferroelectr., Freq. Control*, vol. 63, no. 4, pp. 646–655, Apr. 2016.

[48] H. Leopardi et al., "Single-branch Er: Fiber frequency comb for precision optical metrology with 10^{-18} fractional instability," *Optica*, vol. 4, no. 8, pp. 879–885, Aug. 2017. https://opg.optica.org/optica/abstract.cfm?URI=optica-4-8-879

[49] A. Rolland et al., "Ultra-broadband dual-branch optical frequency comb with 10^{-18} instability," *Optica*, vol. 5, no. 9, pp. 1070–1077, Sep. 2018. [Online]. Available: https://opg.optica.org/optica/abstract.cfm?URI=optica-5-9-1070

[50] M. Giunta, W. Hänsel, M. Fischer, M. Lezius, T. Udem, and R. Holzwarth, "Real-time phase tracking for wide-band optical frequency measurements at the 20th decimal place," *Nature Photon.*, vol. 14, no. 1, pp. 44–49, Jan. 2020.

[51] "Optical-comb-based frequency stability transfer across the spectrum with a multichannel FPGA," Dataset Underlying Publication, doi: 10.5281/zenodo.14249533. Accessed: Jan. 11, 2025.